Structure and function of tomato disease resistance proteins

van Ooijen, G.

Publication date
2008

Chapter 3

Mutational analysis of the MHD motif in resistance proteins reveals its functional role as sensor to transduce nucleotide-dependent conformational changes

Gerben van Ooijen[*], Gabriele Mayr[1*], Mobien M. A. Kasiem, Mario Albrecht[1], Ben J. C. Cornelissen and Frank L. W. Takken

[1] Max Planck Institute for Informatics, Saarbrücken, Germany
*These authors contributed equally to this paper
Published in: Journal of Experimental Botany, 2008, Volume 59, 1383-1397

Resistance (R) proteins in plants are involved in pathogen recognition and subsequent activation of innate immune responses. Most resistance proteins contain a central nucleotide-binding domain, NB-ARC, which is also found in metazoan proteins Apaf-1 and CED-4. In R proteins, this NB-ARC domain consists of three subdomains: NB, ARC1 and ARC2. The NB-ARC domain is a functional ATPase domain, and its nucleotide-binding state is proposed to regulate activity of the R protein. A highly conserved methionine-histidine-aspartate (MHD) motif is present at the carboxy-terminus of ARC2. We report an extensive mutational analysis of the MHD motif in the R proteins I-2 and Mi-1. Several novel autoactivating mutations of the MHD invariant histidine and conserved aspartate are identified. The combination of MHD mutants with autoactivating hydrolysis mutants in the NB subdomain shows that the autoactivation phenotypes are not additive. This finding indicates an important regulatory role for the MHD motif in the control of R protein activity. To explain these observations, a three-dimensional model of the NB-ARC domain of I-2 is built based on the Apaf-1 template structure. The model was used to identify residues important for I-2 function. Substitution of the selected residues, and functional analysis of the mutants, resulted in the expected phenotypes. The hence validated model enables structural and functional interpretation of our mutagenesis results and demonstrates that the MHD motif replaces the sensor II motif found in AAA+ (ATPases Associated with diverse cellular Activities) proteins.

Introduction

To deal with pathogens, plants have evolved an advanced immune system to counteract pathogen-attack. This immune system enables plants to discriminate between self and non-self, and to induce specific defense responses upon pathogen perception. Recognition of non-self can be mediated by so-called Resistance or R proteins (Martin et al., 2003). Upon recognition of specific pathogen-derived molecules, called Avirulence (AVR) proteins, R proteins trigger the induction of plant defenses to restrict pathogen proliferation (Jones and Dangl, 2006). A hallmark of R protein mediated resistance is the hypersensitive response (HR), often visible as a localized cell death response around the infection site.

Over the last decade, many R genes have been cloned and the majority is predicted to encode intracellular multi-domain proteins (Martin et al., 2003; van Ooijen et al., 2007). These R proteins contain a C-terminal Leucine Rich Repeat (LRR) domain fused to a central Nucleotide Binding (NB) domain (NB-LRR proteins). The core nucleotide-binding fold in NB-LRR proteins is part of a larger entity called the NB-ARC domain because of its presence in Apaf-1 (Apoptotic protease-activating factor-1), R proteins and CED-4 (*Caenorhabditis elegans* Death-4 protein) (van der Biezen and Jones, 1998). Structurally related domains, named NACHT (NAIP, CIITA, HET-E and TP1) or NOD (for Nucleotide-Oligomerization Domain), can be found in other animal proteins. Many of these proteins act as receptors sensing intracellular perturbations (Leipe et al., 2004; Ting et al., 2006; Rairdan and Moffett, 2007). Like in R proteins, the NACHT or NOD domains in these proteins are fused to a repeat structure such as an LRR or WD40 repeat (Leipe et al., 2004). The combined activities of the nucleotide-binding domain and the repeat structure probably evolved independently in the plant and animal kingdoms, and might reflect the biochemical suitability of this combination to link ligand recognition with subsequent activation of downstream pathways (Leipe et al., 2004; Ausubel, 2005).

Proteins containing a NB-ARC/NACHT/NOD domain belong to the Signal Transduction ATPases with Numerous Domains (STAND) superfamily (Leipe et al., 2004). It was predicted that the STAND ATPase domain transmits conformational changes, induced by nucleotide exchange or hydrolysis, to other domains of the protein, thereby allowing it to generate a signal (Leipe et al., 2004).

No plant NB-ARC domain crystal structure has been published, but for the human STAND ATPase Apaf-1 such a structure has been solved and was found to contain a bound ADP (Riedl et al., 2005). This 3D structure revealed that the NB-ARC domain is actually composed of four distinct subdomains: the Nucleotide-Binding (NB) fold and ARC1, -2 and -3 subdomains. ARC1 forms a four-helix bundle, ARC2 adopts a winged-helix fold, and ARC3 constitutes another helical bundle. Specific ADP-binding is achieved through eight direct and four H_2O-mediated interactions with various

conserved residues present in the NB, ARC1 and ARC2 subdomains (Riedl et al., 2005). In *C. elegans* CED-4 (Yan et al., 2005) and plant NB-LRR R proteins, ARC1 and ARC2 are conserved, whereas ARC3 is absent (Albrecht and Takken, 2006). Numerous conserved motifs (hhGRExE, Walker A or P-loop, Walker B, GxP, RNBS-A to D, and MHD) have been identified throughout the NB-ARC domain in R proteins (Meyers et al., 1999; Pan et al., 2000) and seem to correspond to residues in Apaf-1 that are involved in nucleotide binding. The functional importance of these motifs is exemplified by the many mutations of motif residues that were demonstrated to result in either loss-of-function or autoactivation of the NB-LRR protein (Grant et al., 1995; Salmeron et al., 1996; Dinesh-Kumar et al., 2000; Tao et al., 2000; Axtell et al., 2001; Bendahmane et al., 2002; Tameling et al., 2002; Tornero et al., 2002; de la Fuente van Bentem et al., 2005; Howles et al., 2005; Tameling et al., 2006; Gabriëls et al., 2007). Autoactivation means that HR is initiated in the absence of pathogen or AVR protein.

The identification of loss-of-function mutations in the nucleotide binding pocket indicated that nucleotide binding is important for NB-LRR R protein function (Tameling et al., 2002). Previous studies in our lab have indeed confirmed that the NB-ARC domain in the R proteins I-2 and Mi-1 binds nucleotides in vitro. This nucleotide binding is required for I-2 function since a P-loop mutant impaired in binding is inactive (Tameling et al., 2002). R proteins have also been demonstrated to hydrolyse ATP in vitro. Two I-2 autoactivating mutants with specific point mutations in the NB subdomain were found to have wild-type nucleotide binding affinities, but to exhibit reduced ATPase activity (Tameling et al., 2006). These observations support a model for R protein function in which the activated state is ATP-bound and the ADP-bound state represents the resting state (Takken et al., 2006; Tameling et al., 2006). Likewise, the ADP-bound state represents the inactive state in Apaf-1 (Riedl et al., 2005). Upon activation, Apaf-1 binds ATP and undergoes conformational changes enabling the formation of an oligomer (Riedl et al., 2005; Riedl and Salvesen, 2007). Regarding NB-LRR R proteins, homo-oligomerization has so far been confirmed only for the tobacco protein N (Mestre and Baulcombe, 2006).

Whereas the NB subdomain forms a catalytic nucleotide-binding and nucleotide-hydrolyzing pocket, our understanding of the role of the adjacent ARC1 and ARC2 subdomains in regulation of R protein activity is limited. No autoactivating mutations have been described in the ARC1 subdomain and only eight loss-of-function mutations are known (Grant et al., 1995; Bendahmane et al., 2002; Tornero et al., 2002). The ARC1 subdomain of the potato NB-LRR protein Rx has been shown to interact with the Rx LRR domain, but also with the heterologous Bs2 and HRT LRR domains when expressed *in trans* (Rairdan and Moffett, 2006). These data suggest that this domain has a structural role and acts as molecular scaffold for LRR binding.

Many autoactivating mutations have been identified in the ARC2 subdomain, the majority of them maps to a highly conserved carboxy-terminal motif named after its consensus sequence methionine-histidine-aspartate, the MHD motif. An aspartate to valine substitution in the MHD motif was first identified by random mutagenesis in Rx and resulted in autoactivation upon transient expression in *N. benthamiana* leaves (Bendahmane et al., 2002). Later on, mutation of D was shown to result in autoactivation in other R proteins like I-2 and L6, (de la Fuente van Bentem et al., 2005; Howles et al., 2005) and in the NB-ARC protein NRC1 (Gabriëls et al., 2007). NRC1 (for NB-LRR protein Required for HR-associated Cell death 1) does not encode an R protein, but is required for induction of HR by several R proteins upon their activation (Gabriëls et al., 2007).

Autoactivating NB-LRR mutants were not only generated by point mutations, but were also obtained by domain swaps between closely related paralogues of Mi-1, Rx, Rp1 and L6 (Hwang et al., 2000; Sun et al., 2001; Howles et al., 2005; Rairdan and Moffett, 2006). Extensive domain-swap studies using Rx and the related Gpa2 protein suggested that the ARC2 subdomain, via its interaction with the LRR, transduces pathogen recognition by the LRR domain into R protein activation (Rairdan and Moffett, 2006). ARC2 thus seems crucial to condition both autoinhibition in the absence of a pathogen, as well as activation of the R protein in the presence of a pathogen.

The strict conservation of the MHD motif in the ARC2 domain across most clades of the STAND superfamily (Leipe et al., 2004) indicates that this motif is important for these molecular functions. Therefore, to gain more insight into a possible key regulatory role of ARC2 and to investigate the role of the MHD motif in more detail, we generated additional mutations in the MHD motif of the R proteins I-2 and Mi-1 and transiently expressed these proteins in *N. benthamiana*. To link the role of the MHD motif to the nucleotide-binding properties of the NB subdomain, double mutants were made that combine the known autoactivation mutations in the NB-subdomain of I-2 to those in the MHD motif.

To further elucidate the molecular role of the MHD motif in R proteins, an in-silico analysis was performed. We chose the crystal structure of Apaf-1 (Riedl et al., 2005) to model the 3D structure of the NB-ARC domain of I-2. Although sequence identity between Apaf-1 and R proteins is low (20%), we could demonstrate that Apaf-1 still represents a suitable template because functionally important residues are well conserved. To validate the model, five residues suggested by the model to be important for function were selected for mutation and were indeed found to be of functional importance for R protein activation. Our 3D model of the NB-ARC domain of I-2 provides a useful additional view of the functional role of the MHD motif and explains the effect of other autoactivating and loss-of-function mutants.

Results

Autoactivating aspartate to valine mutations in the MHD motif of Mi-1 and Rpi-blb1

Mutation of D to V in the MHD motif of the NB-LRR proteins conferring viral (Rx) or fungal resistance (I-2 and L6), and in NRC1, which is required for many R proteins to initiate HR signaling, has been shown to result in autoactivation of these proteins (Bendahmane et al., 2002; de la Fuente van Bentem et al., 2005; Howles et al., 2005; Gabriëls et al., 2007). To examine whether the D to V mutation also results in autoactivation in a nematode, aphid and whitefly resistance protein (Mi-1) and an oomycete resistance protein (Rpi-blb1), we introduced the corresponding mutation in these two proteins. Autoactivation of the mutant proteins was assessed by transient *Agrobacterium tumefaciens*-mediated transformation in five-weeks-old *Nicotiana*

Figure 1
Mutation of the MHD motif aspartate to valine leads to autoactivation. *Nicotiana benthamiana* leaves were agroinfiltrated with constructs to express R proteins mutated in the MHD motif (aspartate to valine). Pictures of representative leaves were taken two (**A**) or four days after agroinfiltration (**B**). **(A)** Counter-clockwise, starting from top-left: Rx^{D460V}, $I\text{-}2^{D495V}$, $Rpi\text{-}blb1^{D475V}$, $Mi\text{-}1^{D841V}$. **(B)** Counter-clockwise, starting from top-left: $Mi\text{-}1^{D841V}$, Rx^{D460V}, $I\text{-}2^{D495V}$, $Rpi\text{-}blb1^{D475V}$.

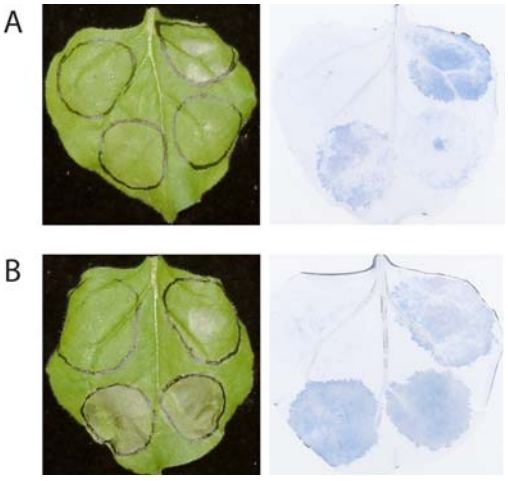

Figure 2
Combination of autoactivation mutations in the NB and ARC2 subdomains. *Nicotiana benthamiana* leaves were agroinfiltrated with constructs to express (mutant) I-2 alleles. Representative leaves were photographed at four days after agroinfiltration. **(A)** Counter-clockwise, starting from top-left: wild-type I-2, $I\text{-}2^{S233F}$, $I\text{-}2^{D283E}$, $I\text{-}2^{S233F/D283E}$. Cell death is visualised by trypan blue staining of the same leaf (right panel). **(B)** Counter-clockwise, starting from top-left: wild-type I-2, $I\text{-}2^{D495V}$, $I\text{-}2^{S233F/D495V}$, $I\text{-}2^{D283E/D495V}$.

benthamiana leaves. Expression of the proteins was driven by the 35S promoter. Pictures were taken at two and four days after agroinfiltration. Figure 1 shows that indeed Mi-1^{D841V} and Rpi-blb1^{D475V} induce a hypersensitive response visible as clear necrosis of the infiltrated sector. The autoactive alleles I-2^{D495V} and Rx^{D460V} are shown as positive controls for HR development. Rx^{D460V} and Rpi-blb1^{D475V} show a rapid HR that is fully developed at two days (Fig. 1A), whereas Mi-1^{D841V} and I-2^{D495V} trigger a slower response that does not lead to a full necrotic sector until three and four days after agroinfiltration, respectively (Fig. 1B). Expression of the wild type protein does not induce HR at the indicated time points (Fig. 2, 4B and data not shown).

The observed autoactivation phenotype of the aspartate-to-valine mutants confirms an important and conserved function for D in the MHD motif of various R proteins conferring resistance to a virus (Rx), a fungus (I-2), an oomycete (Rpi-blb1), and animals (Mi-1). Apparently, mutation of this residue consistently releases R protein autoinhibition, resulting in an autoactivation phenotype or, alternatively, induces another change mimicking the activated state.

Autoactivating mutations in the MHD motif and the NB subdomain do not act synergistically

We have shown previously that the autoactivation phenotype of the I-2^{D495V} mutant depends an a functional nucleotide-binding subdomain since a mutant combining the D495V with the K207R mutation in the P-loop (Walker A) is inactive (Tameling et al., 2006). The K207R mutation in the P-loop of the NB subdomain is a loss-of-function mutation that results in strongly reduced nucleotide-binding capacity (Tameling et al., 2006). Two weak autoactivating mutations in I-2, D283E (in Walker B) and S233F (in RNBS-A), caused reduced ATP hydrolysis rates (Tameling et al., 2006). These mutations are predicted to shift the presumed equilibrium towards the ATP-bound (active) state. Combination of two weak autoactivating mutations in the NB subdomain into a double mutant is therefore predicted to result in an even stronger shift, and hence a more pronounced autoactivation phenotype.

To analyse whether this is the case, the mutations were combined and timing and severity of the HR response after agroinfiltration was scored as a measure for the relative autoactivity of the I-2 mutants. As depicted in figure 2A, combination of both weak autoactivating NB mutations results in a synergetic phenotype. Onset of HR induced by the I-2$^{S233F/D283E}$ double mutant is visible at four days after agroinfiltration on all leaves tested, whereas I-2^{S233F} or I-2^{D283E} single mutants did not show HR at this time point (Fig. 2A). A trypan blue staining of the infiltrated leaf confirms that a weak HR (cell death is visible as blue staining) is induced by the two single mutants, whereas the HR triggered by the double mutant is much more pronounced. The wild-

type I-2 protein does not induce cell death as shown by the absence of any blue colouration. Although the I-2$^{S233F/D283E}$ double mutant is able to induce a clear HR phenotype after four days, the HR is still not as strong as that observed for I-2^{D495V} (Fig. 1), which is in line with an autoinhibitory role of the ARC2 subdomain.

With the NB subdomain being the nucleotide binding and hydrolyzing site, domain swaps of Rx suggest that the ARC2 subdomain, containing the MHD motif, is the regulatory element controlling nucleotide exchange and hence ARC2 activity (Rairdan and Moffett, 2006). Mutating the ARC2 MHD motif might release this autoinhibitory effect on the NB. Combining the MHD mutation with hydrolysis mutations in the NB subdomain would, in this scenario, have a minimal, if any, additive effect on the autoactivation phenotype.

To test this hypothesis, both autoactivating mutations were combined in I-2; the autoactivating mutation D495V in the ARC2 subdomain was paired with either the D283E or S233F in the NB subdomain. As shown in Figure 2B, I-2^{D495V} but not wild-type I-2 induces clear necrosis four days after agroinfiltration. Infiltration of double mutants I-2$^{S233F/D495V}$ and I-2$^{D283E/D495V}$ does not lead to a stronger induction of HR, as confirmed by trypan blue staining of the same leaf (Fig. 2B). Thus, at least visibly, combining the two weak autoactivating mutants with the strong autoactivating D495V mutation in ARC2 does indeed not result in a faster or stronger HR. These data suggest that the MHD motif is a major negative regulatory element controlling the NB subdomain.

Alignment of MHD motifs

Since the D-V mutation of the MHD motif has been found to result in autoactivation of all NB-LRR proteins tested so far, we made an extensive multiple sequence alignment (MSA) of the extended MHD motif of the 50 cloned NB-LRR proteins with confirmed resistance activity, thereby updating a previously published MSA of this region (Howles et al., 2005). For completeness, also the plant NB-LRR proteins NRC1 and NRG1 are included since both are involved in R protein signaling pathways (Peart et al., 2005; Gabriëls et al., 2006). Apaf-1 was included to illustrate the conservation of this motif in a sequence related human protein. The MSA was sorted to match a phylogenetic tree that was generated based on the aligned motifs. Although phylogeny based on such a short sequence is error-prone, clear clusters stand out (Figure 3). This clustering complies with the relationships of R proteins based on the identity of their N-terminal domains. This N-terminal domain contains either predicted coiled-coil (CC) motifs (the CNLs) or shares homology with the *Drosophila* Toll and human Interleukin-1 receptors (TIR, the TNLs) (reviewed in (Martin et al., 2003; van Ooijen et al., 2007)). As can be appreciated from Figure 3, the TNL group (aubergine characters) clusters together and the consensus sequence

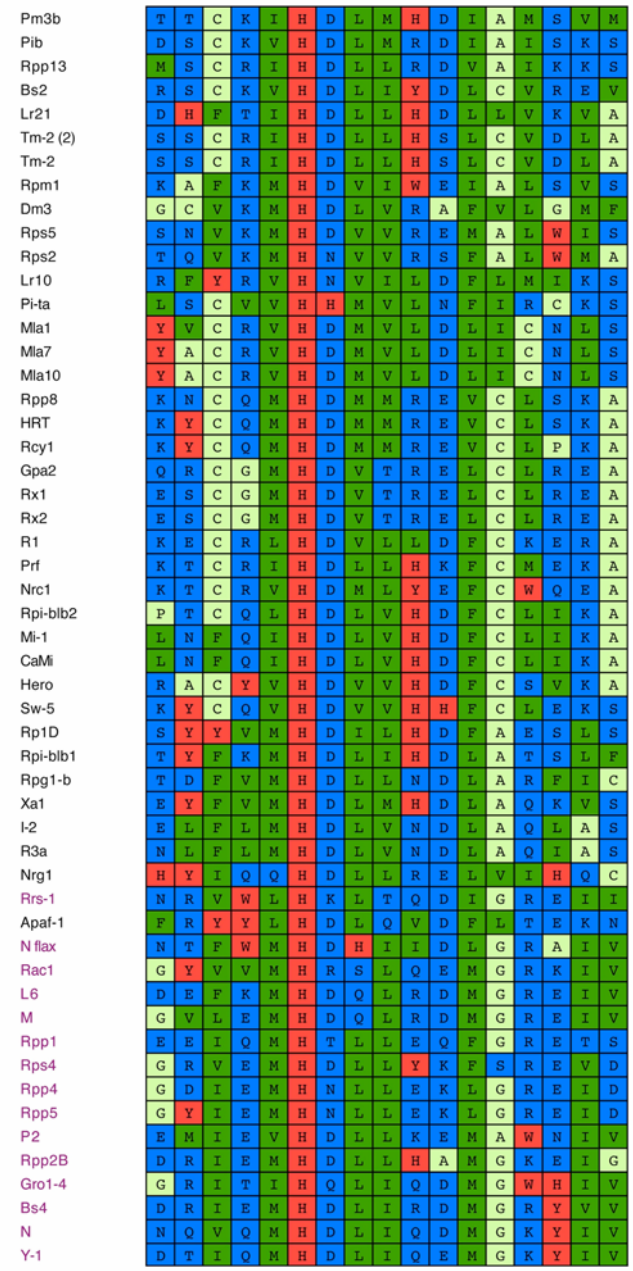

Figure 3

Multiple sequence alignment of the extended MHD motif in 50 R proteins with confirmed resistance activity, the downstream resistance signaling NB-ARC-LRR proteins NRC1 and NRG1, and human Apaf-1. CC-NB-LRR proteins are marked in blue, and TIR-NB-ARC-LRR proteins in red. Amino acid residues are colored based on their chemical type; beige: small hydrophobic (A, C, G, P), blue: hydrophilic (D, E, K, N, Q, R, S, T), red: aromatic (H, W, Y), green: large hydrophobic (F, I, L, M, V). TNLs are marked in aubergine.

of its MHD motif is C-terminally elongated compared to those of CNLs. The conservation of this motif in human Apaf-1 is clear as well.

As can be deduced from the MSA in Figure 3, the most conserved residue in the MHD motif is the histidine that is invariable in all NB-LRR R proteins. The histidine is always N-terminally flanked by a hydrophobic residue (a methionine in 53% of the cases), whereas the C-terminal neighbouring residue is an aspartate in most cases (83%). This means that, although conservation of the aspartate is considerable, it is not invariant. The histidine is the only invariable residue in the MHD motif, which suggests an essential role for this residue.

Table 1 Substitutions of I-2 H494

Amino acid		No. of clones	Phenotype
A	Alanine	5	+++
C	Cysteine	1	++
D	Aspartic acid	8	++
E	Glutamic acid	2	++
G	Glycine	10	++
K	Lysine	3	++
N	Asparagine	1	++
R	Arginine	13	++
S	Serine	7	++
T	Threonine	7	++
V	Valine	6	++
M	Methionine	2	+
Y	Tyrosine	4	+
F	Phenylalanine	4	+/-
P	Proline	3	+/-
L	Leucine	12	-
Q	Glutamine	5	-
W	Tryptophan	1	-
I	Isoleucine	0	nd
H	Histidine	85	-
*	stop	5	-

Mutation of the histidine in the MHD motif

Because the histidine is the most conserved residue in the MHD motif of plant NB-LRR R proteins, we decided to analyze the effect of mutating this residue on I-2 function. We first generated a small library of I-2 clones that encode proteins that are variable for residue H494. This library was made by site-directed mutagenesis using the megaprimer method (Ke and Madison, 1997). In the mutagenic primer, the H494-encoding codon (CAT) was replaced for NNS (in which N can be any nucleotide and

S can be either G or C). Introduction of S reduces the number of possible codons to 32, thereby increasing the relative percentage of the single-codon amino acids tryptophan and methionine. To have a good representation of all possible codons, an approximately six-fold excess of the 32 possible codons (184 clones) was sequenced. The obtained variants, and the number of clones coding for each amino acid at position 494, are shown in Table 1. Of the 19 possible amino acid replacements plus three stop codons, isoleucine was the only one that was not present in the sequenced set of clones. An overrepresentation of the wild-type histidine residue was obtained, probably due to inefficient removal of the wild-type insert.

The phenotype of the H494 variants was analyzed by transient expression in *N. benthamiana* leaves using agroinfiltration and assessment of timing and extent of cell death of the infiltrated region. Except for the stop codon mutants and the wild-type, we did not observe HR either when a glutamate, leucine or tryptophan replaced the histidine at position 494. The 15 other replacements resulted in autoactivation. However, variation in the amplitude of timing and intensity of HR was observed (Table 1). The results in Table 1 represent the average observed effects of at least two independent clones where possible. HR was ranked from very strong (+++) to no visual effect (-). To illustrate the range of HR, Figure 4A shows I-2 mutants H494A (+++), H494R (++), H494V (+), H494F (+/-), H494L (-) and H494Q (-). The same activity range is also evident upon trypan blue staining of this leaf (Fig. 4A, right panel). Substitution of H494 for alanine reproducibly resulted in the fastest induction of HR. Limited cell death was also visualised upon expression of I-2^{H494L} and I-2^{H494Q}, suggesting that the latter two could still weakly autoactivate. However, since the intensity of the blue staining is comparable to that for wildtype I-2, it likely represents background staining.

To investigate whether corresponding mutations in a related NB-LRR protein, Mi-1, confer similar phenotypes as obtained for I-2, we generated Mi-1 MHD motif mutants H840A, H840R, H840V, H840Q and as a negative control H840stop. Similar to I-2, Mi-1^{H840A} leads to the strongest autoactivation (Fig. 4B), whereas Mi-1^{H840R} and Mi-1^{H840V} show intermediate phenotypes. Wild-type Mi-1 and Mi-1^{H840Q} do not induce HR, but induce a similar light blue staining as the Mi-1^{H840stop} control.

Autoactivation by Mi-1 MHD mutants is not due to higher expression levels in the plant

To test whether autoactivation induced by mutations in the MHD are due to differences in protein expression levels rather than a direct effect of the mutation, the expression levels of the various mutants were analyzed. To detect the R proteins after *in planta* expression, antibodies against I-2 and Mi-1 were raised in rabbit.

Either a synthetic I-2 peptide or the Mi-1 NB-ARC domain with part of its N-terminal flanking sequence (Mi-1 amino acids 161-899) were used as antigen. The latter recombinant Mi-1 protein was heterologously produced in *E. coli* as described in the Methods section. Using affinity purified I-2 antibodies, we were unable to detect the R protein in protein extracts isolated from agroinfiltrated *N. benthamiana* leaves, although the antibody successfully recognized *E. coli*-produced I-2 protein (data not shown). These results indicate that I-2 expression levels *in planta* are probably below the detection level of the I-2 antibody (data not shown and (Tameling et al., 2006)). Efforts to detect N- or C-terminally epitope-tagged I-2 failed and since all tags tested rendered the autoactivation mutant I-2^{D495V} inactive, these efforts where not continued.

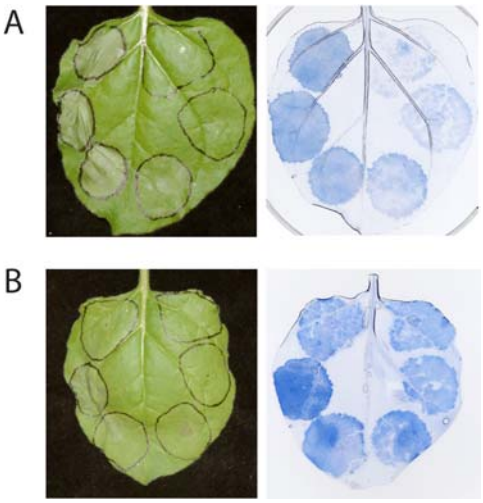

Figure 4

Mutation of the MHD motif histidine leads to a range of autoactivating phenotypes. *Nicotiana benthamiana* leaves were agroinfiltrated with constructs to express I-2 or Mi-1 mutants variant for the MHD motif histidine. (**A)** I-2 mutants variant for H494. Counter-clockwise, starting from top-left: I-2^{H494A}, I-2^{H494R}, I-2^{H494V}, I-2^{H494F}, I-2^{H494L}, I-2^{H494Q}. Picture was taken four days after agroinfiltration. Cell death is visualised by trypan blue staining of the same leaf (right panel). (**B)** Mi-1 mutants variant for H840. Counter-clockwise, starting from top-left: wild-type Mi-1, Mi-1^{H840A}, Mi-1^{H840R}, Mi-1^{H840V}, Mi-1^{H840Q}, Mi-1^{H840stop}. Picture was taken four days after agroinfiltration. Cell death is visualised by trypan blue staining of the same leaf (right panel).

In contrast to I-2, *in planta* produced Mi-1 could readily be detected using the Mi-1 antibody. The Mi-1 antibody detects both full-length Mi-1 and a truncated version lacking the LRR in total protein extracts from *N. benthamiana* leaves, following transient expression using agroinfiltration (Supplemental Fig. S1). No Mi-1-specific bands were detected on western blots from protein extracts of leaves agroinfiltrated with Mi-1 LRR (amino acids 900-1257), showing specificity of the antibody for the N-terminal part of Mi-1. Besides the Mi-1 protein, a ~80 kDa band was consistently found in all *N. benthamiana* extracts, including these from non-infiltrated leaves. The nature of this *N. benthamiana* specific protein is not known, but like Mi-1 it was not recognised on blots incubated with pre-immune serum (Supplemental Fig. S1). To analyze the expression levels of Mi-1 mutants, constructs encoding Mi-1^{D841V} and H840 mutants showing strong (H840A), intermediate (H840V) or no (H840Q)

autoactivating phenotype were agroinfiltrated. Infiltrated leaves were harvested after 24 hours, well before onset of HR, and subsequently used for total protein extraction. For comparison, the expression level of wild-type Mi-1 was included. A western blot of total soluble protein from agroinfiltrated leaves was stained with Ponceau S to confirm equal loading. This blot was subsequently probed with the Mi-1 antibody and Figure 5 shows the Mi-1 variants migrating at the predicted weight of ~145 kDa. The expression levels of autoactivating mutants do not differ significantly from the wild-type control. These results substantiate that induction of HR by Mi-1 mutants is not caused by differences in protein level and can solely be attributed to the specific mutations.

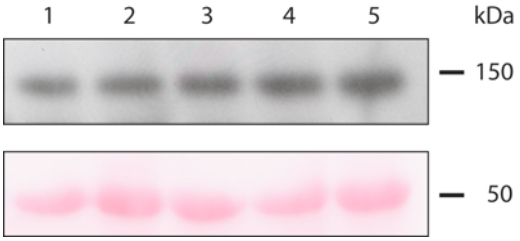

Figure 5 – Expression levels of wild-type and mutant Mi-1. *Nicotiana benthamiana* leaves were agroinfiltrated with constructs to express (mutant) Mi-1. One day after agroinfiltration, protein extracts were subjected to SDS-PAGE followed by Ponceau S staining of Rubisco **(B)** and immunoblotting with anti-Mi **(A)**. 1: Mi-1 wild-type, 2: Mi-1^{D841V}, 3: Mi-1^{H840A}, 4: Mi-1^{H840V}, 5: Mi-1^{H840Q}.

Structure-based multiple sequence alignment of R proteins

To provide an explanation for the phenotypes of the MHD mutants, a 3D model of the I-2 NB-ARC domain was built. To construct the structure model, we first examined sequence conservation and domain organization of R proteins by generating a structure-based multiple sequence alignment (Fig. 6). Two homologous proteins with known structure, human Apaf-1 and *C. elegans* CED-4, were included (Riedl et al., 2005; Yan et al., 2005). The initial alignment was refined manually, taking into account secondary structure predictions of R proteins, and known structure assignments of Apaf-1 and CED-4. Sequence identity between I-2 and Apaf-1 NB-ARC domains is low (24%) and concentrated within or adjacent to conserved motifs present in the three subdomains of the NB-ARC domain of R proteins (Fig. 6).

As can be seen in Figure 6, most known R protein motifs are also conserved in Apaf-1 and CED-4. The most important exception is the MHD motif itself, which is conserved in Apaf-1 but not in CED-4. The RNBS-C motif is not conserved either in CED-4 and has very low conservation in Apaf-1. Only two residues of this motif are in common with R proteins. The RNBS-D is conserved neither in CED-4 nor in Apaf-1. In the Apaf-1 crystal structure, the corresponding region is not involved in formation of the ADP binding pocket and is located on a helix within ARC2. Another remarkable

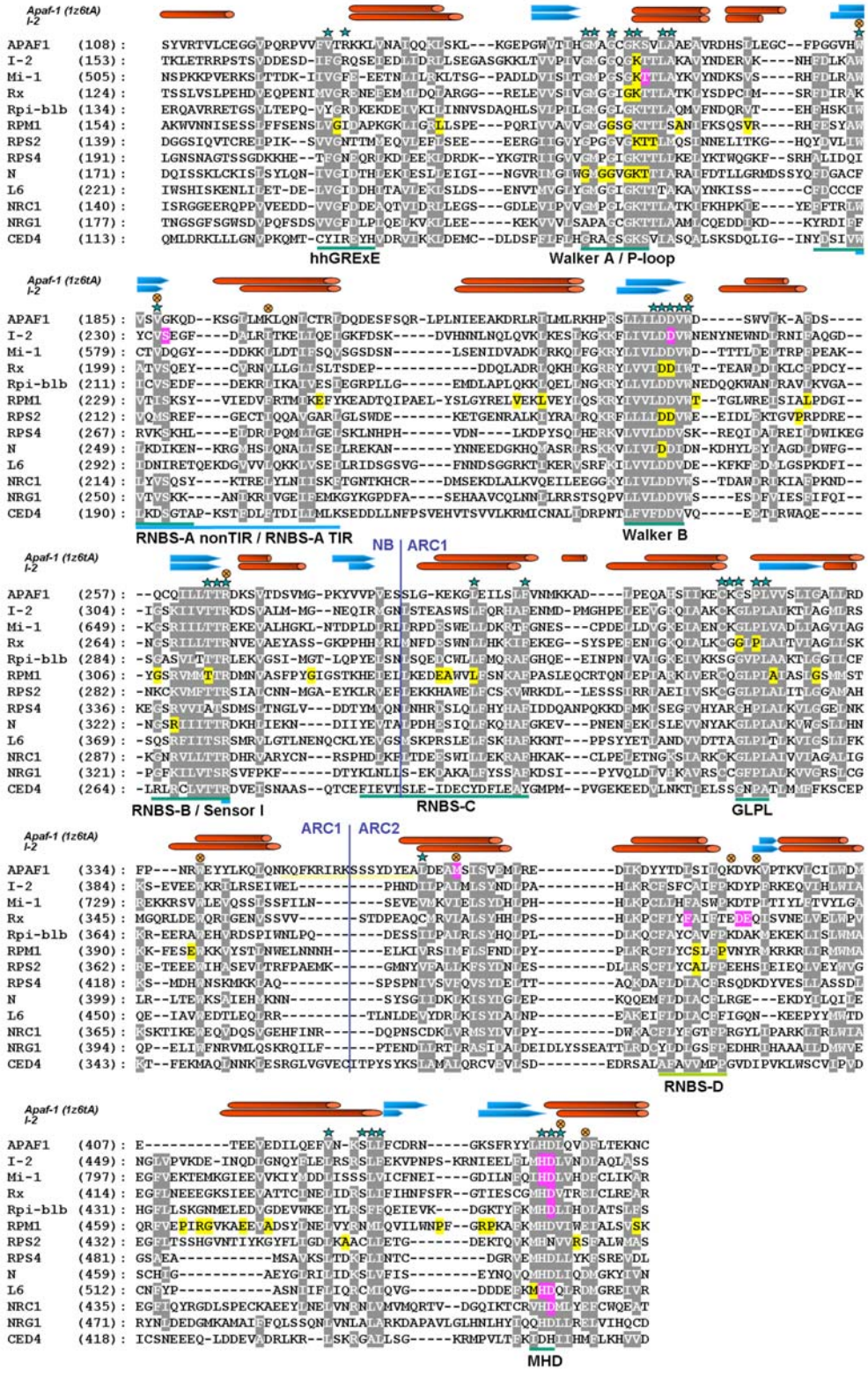
Apaf-1 (1z6tA)
I-2
APAF1 (108) :
I-2 (153) :
Mi-1 (505) :
Rx (124) :
Rpi-blb (134) :
RPM1 (154) :
RPS2 (139) :
RPS4 (191) :
N (171) :
L6 (221) :
NRC1 (140) :
NRG1 (177) :
CED4 (113) :
hhGRExE
Walker A / P-loop
APAF1 (185) :
I-2 (230) :
Mi-1 (579) :
Rx (199) :
Rpi-blb (211) :
RPM1 (229) :
RPS2 (212) :
RPS4 (267) :
N (249) :
L6 (292) :
NRC1 (214) :
NRG1 (250) :
CED4 (190) :
RNBS-A nonTIR / RNBS-A TIR
Walker B
NB | ARC1
APAF1 (257) :
I-2 (304) :
Mi-1 (649) :
Rx (264) :
Rpi-blb (284) :
RPM1 (306) :
RPS2 (282) :
RPS4 (336) :
N (322) :
L6 (369) :
NRC1 (287) :
NRG1 (321) :
CED4 (264) :
RNBS-B / Sensor I
RNBS-C
GLPL
ARC1 | ARC2
APAF1 (334) :
I-2 (384) :
Mi-1 (729) :
Rx (345) :
Rpi-blb (364) :
RPM1 (390) :
RPS2 (362) :
RPS4 (418) :
N (399) :
L6 (450) :
NRC1 (365) :
NRG1 (394) :
CED4 (343) :
RNBS-D
APAF1 (407) :
I-2 (449) :
Mi-1 (797) :
Rx (414) :
Rpi-blb (431) :
RPM1 (459) :
RPS2 (432) :
RPS4 (481) :
N (459) :
L6 (512) :
NRC1 (435) :
NRG1 (471) :
CED4 (418) :
MHD

Figure 6
Structure-based multiple sequence alignment of the NB, ARC1 and ARC2 subdomains of NB-LRR R proteins, Apaf-1 and CED-4. The secondary structure assignment of the Apaf-1 protein (PDB code 1z6t, chain A) and the secondary structure prediction of I-2 are depicted at the top of the alignment (beta-strands in blue, alpha-helices in red). Domain borders are indicated as vertical blue lines. Motifs are annotated as horizontal green and blue lines below the aligned sequences. Amino acid positions experimentally shown to lead to an HR response are highlighted in pink, loss-of-function mutations in yellow. Amino acids located in the ADP binding site of Apaf-1 and well-conserved in R proteins are marked by green stars. Residue positions of potential interest for experiments are marked by orange crossed circles.

difference between Apaf1/CED-4 and R proteins is a loop connecting the ARC1 and ARC2 subdomains, which is considerably shorter in R proteins. Despite these differences, we observe a remarkable conservation of the residues forming the nucleotide binding pocket. This is illustrated in Figure 6, where all residues are marked that are conserved in R proteins and located in the Apaf-1 ADP binding pocket. Most of these amino acids are located in previously defined motifs, except for Apaf-1 serine 422 in the ARC2 subdomain. This serine participates in a water-mediated hydrogen bond to the ADP ribose. A direct hydrogen bond with the β-phosphate of ADP was observed for histidine 438 in the Apaf-1 MHD motif (Riedl et al., 2005). These two important amino acids as well as most of the other conserved ADP binding pocket residues are missing in CED-4. The ARC2 subdomain in R proteins is generally more similar to Apaf-1 than to CED-4. In conclusion, the conserved cluster of residues in the ADP binding pocket make the Apaf-1 ADP bound structure the preferable modelling template for the NB-ARC domain of R proteins.

Protein structure model of I-2 and localization of mutations

Based on the multiple sequence alignment (Fig. 6), we propose a similar secondary structure and a conserved 3D arrangement of protein subdomains and nucleotide binding mode in the NB-ARC domain of R proteins as found for ADP-bound Apaf-1. Therefore, this Apaf-1 crystal structure (PDB code 1z6t, chain A) was chosen as modelling template for I-2 (Fig. 7 and S2). As in case of the Apaf-1 NB-ARC domain, in the NB-ARC structural model of I-2 the ADP molecule is deeply buried in a pocket formed at the interface of the NB, ARC1 and ARC2 subdomains.

Mapping of known loss-of-function mutations identified in the NB-ARC domains of R proteins onto the I-2 structural model reveals that they are located at many different positions scattered throughout the molecule (Fig. 6, motifs indicated in Fig. 7, and (Takken et al., 2006)). When located in the ADP binding pocket, the loss-of-function mutations point to the adenosine binding site of the pocket, possibly affecting ADP

binding. This observation agrees well with the finding that nucleotide binding is essential for R protein function (Tameling et al., 2006).

In contrast to loss-of-function mutations, autoactivating mutations are exclusively located on the opposite side of the interface between the NB and ARC2 subdomains. Here, they map in, or close to, the ADP binding pocket where they are located near the phosphates, which suggests a role in phosphate binding and/or hydrolysis (Fig. 7). This is in good agreement with the observation that hydrolysis mutants are autoactivating (Tameling et al., 2006).

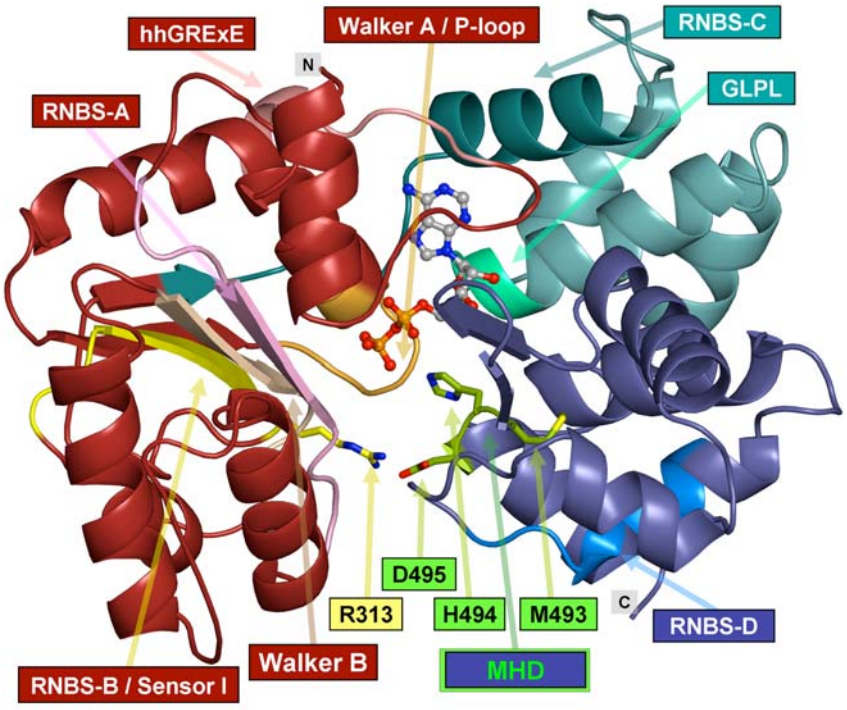

Figure 7

Computationally derived 3D structure model of the NB-ARC domain of the resistance protein I-2. The model was created using the ADP bound structure of human Apaf-1 (PDB code 1z6t, chain A) as structural template for I-2. The locations of R protein motifs are marked with arrows. Amino acids of the MHD motif as well as the sensor I arginine are shown in stick representation. ADP atoms are depicted as balls-and-sticks. Subdomain coloring is: NB: red, ARC1: green, ARC2: blue. Atom coloring is: oxygen: red, nitrogen: blue, phosphorus: orange.

Specific point mutations validate the I-2 NB-ARC structure model

The observed clustering of autoactivating mutations suggests that the model depicted in Figure 7 is a reliable representation of the NB-ARC domain of R proteins. Using this model, residues can be identified that, based on their structural position in the 3D structure, are important for R protein activity. Based on the model, we

selected five mutations at predicted important structural positions (Fig. S2). One mutation (R313A) was made in the sensor I motif and is a predicted loss-of-function mutant. Three mutations were made at the interface of the NB and ARC2 (i.e. W229A, V232A and W285A). One mutation, S474A, was made outside this interface and is not predicted to be of importance and thus should not effect R protein function. As can be seen in Figure 8A, expression of the I-2^{R313A} sensor I mutant induces less cell death (visualised by trypan blue) than expression of wild-type I-2 from the same binary vector. This observation suggests that the mutant is incapable of inducing cell death and might represent a loss of function mutant. Of the other 3 mutants with predicted functional relevance, I-2^{V232A} was found to represent an autoactivation mutant triggering clear HR (Fig. 8B), whereas W229A and W285A represent likely loss-of-function mutants (Fig. 8C and D). As expected, the I-2^{S474A} mutant is indeed neither gain- nor loss-of-function as it shows similar cell death levels like the wild-type I-2 protein (Fig. 8E).

These results support the validity of the NB-ARC model presented in Figure 7, and corroborates its use to derive a molecular function for the MHD motif as discussed below.

Discussion

The central NB-ARC domain in R proteins has been proposed to function as a molecular switch that defines the activation state of the protein depending on the nucleotide bound (Rairdan and Moffett, 2006; Takken et al., 2006; Tameling et al., 2006). In this functional model, the NB subdomain is the primary nucleotide binding and hydrolysis pocket, the ARC1 subdomain is required for the intramolecular interaction with the LRR, and the ARC2 subdomain transduces pathogen perception by the LRR into R protein activation (Rairdan and Moffett, 2006; Tameling et al., 2006). To examine how the ARC2 regulates R protein activity, we focused on the MHD motif in this subdomain. The results presented here indicate that the histidine in the MHD motif is a key component of the 'switch' of R protein activity.

Functional roles of the MHD residues

Both the histidine and the aspartate in the MHD motif are among the most conserved residues in R proteins, pointing to an important functional and structural role (Fig. 3 and 7). As part of a framework of conserved amino acids in the deeply buried ADP binding pocket, the histidine is in an apparently critical position (Fig. 7). This location suggests that it fulfils the same role as proposed for the corresponding histidine in Apaf-1, which is to directly bind and position the β-phosphate of the ADP (Riedl et al., 2005; Albrecht and Takken, 2006). Such a direct interaction of the winged-helix domain with the nucleotide is a unique feature of Apaf-1 and is not found in related

AAA+ ATPases (Riedl et al., 2005). The latter use a conserved arginine residue in the so-called sensor II motif in the helical bundle (corresponding to the ARC1 subdomain) to coordinate the bound nucleotide and control intersubunit interactions (Ogura et al., 2004). The region around the conserved arginine is referred to as sensor II by analogy with an arginine in adenylate kinases that mediates conformational changes upon ATP binding (Müller and Schulz, 1992; Guenther et al., 1997). Unlike in the AAA+ proteins, no sensor II motif is present in STAND proteins like Apaf-1 and R proteins. In Apaf-1, the binding of H438 to the beta-phosphate of the ADP stabilizes the compact closed conformation of the NB-ARC domain (Riedl et al., 2005). Through ADP binding, the histidine and serine participate in the interaction between the NB and the ARC2 subdomains. Mutation of the MHD histidine and aspartate may weaken ADP–protein and inter-subdomain interactions resulting in the destabilization of the closed ADP-bound conformation. Consequently, nucleotide exchange could be favoured, resulting in a constitutively active conformation of the R protein. In this way, the MHD motif takes over both AAA+ protein sensor II functions; coordination of the bound nucleotide and control of intersubunit interactions. Such a major positive regulatory role for the MHD is in line with the observation that combining an MHD mutant with a NB hydrolysis mutant does not result in a faster HR response (Fig. 2).

A sensor II function for the MHD motif could also explain the autoactivating phenotype obtained upon mutation of the aspartate. This aspartate is located C-terminally of the histidine at the positively charged end of an alpha-helix, a position preferably occupied by negatively charged amino acids stabilising the helix dipole. Mutating the aspartate or any other residue present at this position (Fig. 3) might reposition the helix, thereby dislocating the preceding histidine and weakening its interaction with the ADP.

In an ADP-bound conformation, the MHD aspartate may contact the so-called sensor I arginine through a salt bridge (as predicted by the WHAT-IF server). This conserved arginine (Apaf-1 R265, corresponding to R313 in I-2 (Fig. 7)) in the sensor I motif senses the presence of a γ-phosphate on the bound nucleotide in related AAA+ proteins and relays this information to other domains of the protein (Ogura and Wilkinson, 2001). Because only the ADP bound structure has been solved for Apaf-1, it is not known how it senses a γ-phosphate, but the corresponding arginine directly interacts with the γ-phosphate in the crystal structure of ATP-bound CED-4 (Yan et al., 2005). The sensor I maps to the NB subdomain and is hallmarked by the hhhhToR signature, which is referred to as the RNBS-B motif in plant R proteins ((Meyers et al., 1998) and Fig. 6). The importance of this motif was suggested by loss-of function mutations of the two neighboring threonine amino acids in Rpm1 and Prf ((Salmeron et al., 1996; Tornero et al., 2002) and Fig. 6), which could result in a

side chain dislocation of the adjacent sensor I arginine. Direct proof for functional importance of the sensor I arginine was shown by substitution for an alanine. As shown in Figure 8A, this mutation results in a loss-of-function phenotype. In light of this, mutation of the MHD aspartate might not only directly affect ADP binding through a delocalization of the preceding histidine, but could also lead by itself to a more open conformation of the NB-ARC as it can no longer interact with sensor I. An open conformation would result in weaker binding of ADP, allowing exchange for ATP and resulting in R protein activation.

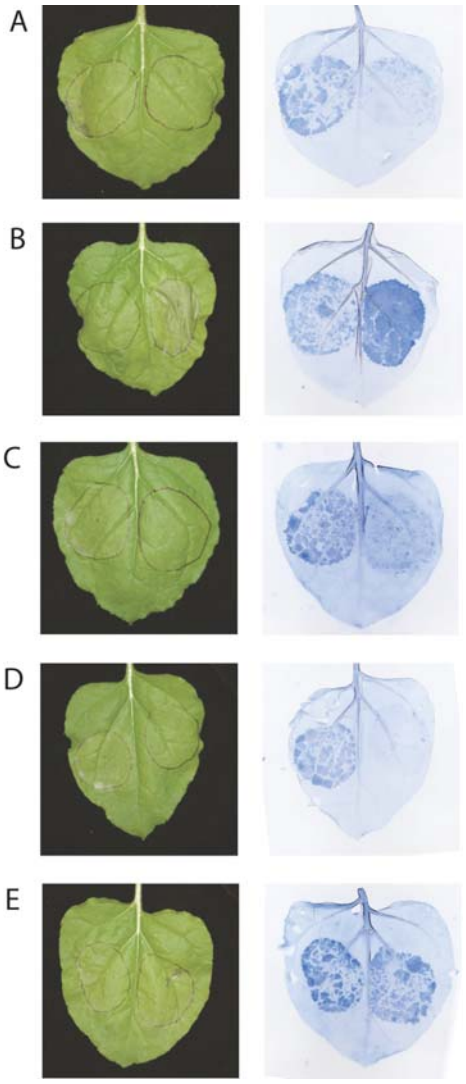

Figure 8
Mutation of predicted important residues alters R protein function. *Nicotiana benthamiana* leaves were agroinfiltrated with constructs to express wild-type or mutant I-2 protein. After pictures were taken (left panels), the same leafs were stained for cell death using trypan blue (right panels). Wild-type I-2 is expressed in the left leaf half, mutants in the right. **(A)** I-2^{R313A} **(B)** I-2^{V232A}, **(C)** I-2^{W229A}, **(D)** I-2^{W285A}, **(E)** I-2^{S474A}.

To conclude, the MHD histidine may be in direct contact with the ADP, and its mutation could directly destabilize the inactive ADP-bound protein complex, allowing nucleotide exchange and activation of the protein. Mutation of the aspartate could both dislocate the histidine making it less effective in repressing the R protein and/or negatively influence the interaction between the NB and ARC2 subdomains, thereby destabilizing the closed, inactive protein conformation.

Implications of the I-2 structural model on residues outside the MHD motif

The availability of a structural model of the NB-ARC domain of R proteins allows the formation of hypotheses on the molecular mechanism underlying autoactivation

phenotypes induced by mutation of residues outside the MHD motif. Most auto-activating mutations in R proteins map to the interface of the NB and the ARC2 subdomains, such as I-2^{S233F}, I-2^{D283E}, Rx^{D399V} and Rx^{E400K} (Bendahmane et al., 2002; Tameling et al., 2006). Our structural model of I-2 shows that I-2 residues S233 and D283 are on the same side of the NB subdomain and are facing Rx residues D399 and E400, which are located on the opposite side, on the ARC2 subdomain.

I-2 mutations S233F and D283E in the NB subdomain (Supplemental Fig. S2) have been shown to reduce the ATP hydrolysis rate (Tameling et al., 2006). Rx residues D399 and E400 in Rx (Bendahmane et al., 2002) are relatively distant from the ATP. These residues are therefore unlikely to be directly involved in ATP hydrolysis. These ARC2 residues, however, contact the residues in the neighbouring NB subdomain and may thus be involved in stabilizing the inactive domain complex. Mutation of these residues may destabilize the inactive conformation, allowing the protein to adopt its activated state. This hypothesis is in agreement with the assumption that STAND ATPases like R proteins undergo conformational changes upon activation (Moffett et al., 2002; Leipe et al., 2004; Rairdan and Moffett, 2006; Takken et al., 2006; Bent and Mackey, 2007; van Ooijen et al., 2007).

The observed clustering of known mutations in our structural model allowed identification of additional mutations that should affect protein function (Fig. 6). These residues are amino acids that are well-conserved and also in the spatial vicinity of experimentally verified sites. Their 3D locations are depicted in the structural model of I-2 (Supplemental Fig. S2). Two conserved residues were selected in the RNBS-A (W299A and V232) because of their predicted positions at the interface between NB and ARC2. Transient expression of the V232A resulted in autoactivating and an intense blue staining upon trypan blue staining (Fig. 8B). This observations supports the hypothesis that this loop is important for interactions between these two subdomain. The W229A mutant was shown to induce less cell death than wild-type I-2, suggesting that it is either hypoactive or inactive (Fig. 8C). In the NB-ARC structure (Supplemental Fig. S2), this tryptophan is deeply buried and has numerous non-covalent interactions with other amino acids, e.g. the Walker B D282. Mutation likely abrogates the stability of the protein fold leavind a non-functional protein.

W285 in the Walker B motif was selected because of its position near the aspartates that are required for ATPase activity. Mutation of this residue resulted in an inactive or hypoactive protein, confirming that this residue is important for function (Figure 8D).

An intriguing difference between R proteins and Apaf-1 as well as CED-4 is the loop connecting ARC1 and ARC2. In CED-4, this loop harbours a tyrosine that, together with the sensor I arginine and the P-loop lysine, is crucial for coordinating the gamma-phosphate of ATP (Yan et al., 2005). Likely, this loop is flexible, enabling

ARC2 dislocation upon activation. The loop is of variable length, but considerably shorter in R proteins (Fig. 6 and Supplemental Fig. S2) and also lacks sequence conservation. In the Apaf-1 structure, the loop covers part of the interface between the NB and ARC2 subdomains and is involved in interdomain re-organization upon activation. This implies that even though the proposed ADP-bound conformation of the NB-ARC domain in R proteins is similar to that of APAF-1, the ATP-bound state might differ.

In conclusion, our data support the current models for R protein function in which the NB-ARC acts as a molecular switch (Takken et al., 2006; Tameling et al., 2006; Bent and Mackey, 2007; van Ooijen et al., 2007). Although a crystal structure is required to confirm the provided 3D model, it can already serve as a framework for the formulation of hypotheses on how mutations exert their effect. This structural model provides insight into the function of the conserved elements within the NB-ARC domain and sheds light on the molecular mechanisms through which R proteins orchestrate plant defence.

ACKNOWLEDGEMENTS

We like to thank Harold Lemereis and Ludek Tikovski for plant handling. Thijs Hendrix is acknowledged for raising the Mi-1 antibody. Martijn Rep is acknowledged for critical review of the manuscript. pKG6210 containing the Mi-1 genomic region was provided by Keygene N.V., The Netherlands. A construct containing the Rpi-blb1 gene was kindly provided by Dr. E. van der Vossen, Wageningen University, Wageningen, The Netherlands.

G.v.O. is supported by the Research Council for Earth and Life Sciences (ALW) with financial aid from the Netherlands Organization for Scientific

Research (NWO). G.M. and M.A. have been financially supported by the German National Genome Research Network (NGFN). The research has been conducted in the context of the BioSapiens Network of Excellence funded by the European Commission under grant number LSHG-CT-2003-503265.

Materials and methods

Construction of vectors

Wild-type I-2 (wp42) and derived mutants D495V (wp45), S233F (wp54) and D283E (wp60) in pGreen (Hellens et al., 2000) have been described (Tameling et al., 2002; de la Fuente van Bentem et al., 2005; Tameling et al., 2006). All oligonucleotides (marked FP) used in this study were purchased from MWG, Germany, and can be found in Table 2. I-2^{D495V} was combined with I-2^{S233F} or I-2^{D283E} by swapping a 0.8 kb *Sal*I/*Bam*HI fragment from wp54 and wp60 into wp45. To make the double I-2$^{S233F/D283E}$ mutant a 3-points ligation was performed; wp45 was digested with *Sal*I/*Acc*65I and fragments of wp60 (*Acc*65I/*Bst*XI) and wp54 (*Sal*I/*Bst*XI) were inserted to obtain I-2$^{S233F/D283E}$.

To generate the H494 mutant library the I-2 coding sequence was PCR amplified from wp42 using primers FP794 and FP796 and gateway *att*B flanks were introduced in a second amplification using FP872 and

FP873. The resulting PCR product was recombined into pDONR207 (Invitrogen) via a Gateway BP clonase (Invitrogen) reaction to obtain pMK13. To establish random mutagenesis of residue 494, a degenerate primer FP1158 containing NNS as a codon for residue 494 was used in combination with FP490. The obtained 336 bp PCR product was subsequently used as a mutagenic megaprimer (Ke and Madison, 1997) in combination with FP216, to amplify a 0.8 kb fragment from wp42. This fragment was digested with *Bam*HI/*Nde*I and ligated into pMK13 using the same sites and subsequently recombined to binary vector CTAPi (Rohila et al., 2004) using a Gateway LR reaction (Invitrogen, Carlsbad, USA). Because the I-2 sequence contains its endogenous stop codon there is no translational fusion to the TAP tag. pMK13 was used as a template for circular mutagenesis (Hemsley et al., 1989) to generate I-2 mutants W229A, V232A, W285A, R313A, and S474A using primer pairs FP1834/FP1835, FP1836/FP1837, FP1838/FP1839, FP1840/FP1841, FP1844/FP1845, respectively. The resulting mutant isoforms were subsequently recombined to CTAPi (Rohila et al., 2004) by a Gateway LR reaction (Invitrogen). Creation of pSE23, a binary construct containing Mi-1 under control of its endogenous promoter, and the Mi-1^{T557S} mutation is described before (Gabriëls et al., 2007). The coding sequence of Mi-1, including its stop codon and intron, was amplified from pSE23 by PCR using primers FP764 and FP766, and Gateway *att*B flanks were added by adapter PCR using primers FP872 and FP873. The PCR product was transferred to binary vector CTAPi (Rohila et al., 2004) by the Gateway one-tube protocol for cloning *att*B-PCR products directly into destination vectors (Invitrogen) to create pG74. Mi-1 D841V was generated using pG74 as a template for mutagenic overlap extension PCR (Higuchi et al., 1988) using primer sets FP860/FP873 and FP861/FP872. Likewise, the constructs containing Mi-1 H840R,

Tab2 Oligonucleotide sequence

FP	Sequence
211	ctggtcgaccaaccataatgctacttaaataagg
216	gacatgcatttgaaaacatgg
490	taatccatgtccgagaaata
754	caagatgcatgttctcatcc
755	catacaggttcaagtatc
756	ccacctgtctaactcatccactaccc
764	aaaaagcaggctctatggaaaaacgaaaagatatt
766	agaaagctgggttctacttaaataaggggatattctt
771	aaaaagcaggctctatggctgaagctttcatt
793	agaaagctgggttttaaatatatatattcacattag
794	aaaaagcaggctctatggagattggcttagcag
796	agaaagctgggttttaaatatatttccaatcgata
860	ccaaattcatgttcttgtgcatga
861	gtcatgcacaagaacatgaatttgg
872	ggggacaagtttgtacaaaaaagcaggct
873	ggggaccactttgtacaagaaagctgggt
1095	cgggatcccatgggttgatactgaatgg
1099	gtatgccgggttcaggtgcagcaactttggcatacaaagtatac
1100	gatatactgaatttccaaattgctgatcttgtgcatgacttttg
1102	gtatactttgtatgccaaagttgctgcacctgaacccggcatac
1103	caaaagtcatgcacaagatcagcaatttggaaattcagtatatc
1158	gaggaattattccttatgnnsgaccttgtcaatgatttag
1541	ctgaatttccaaattcttgatcttgtgcatgac
1542	gtcatgcacaagatcaagaatttggaaattcag
1543	ctgaatttccaaattcgtgatcttgtgcatgac
1544	gtcatgcacaagatcacgaatttggaaattcag
1545	ctgaatttccaaattgttgatcttgtgcatgac
1546	gtcatgcacaagatcaacaatttggaaattcag
1547	ctgaatttccaaatttaggatcttgtgcatgac
1548	gtcatgcacaagatcctaaatttggaaattcag
1598	ctgaatttccaaattcaggatcttgtgcatgac
1599	gtcatgcacaagatcctgaatttggaaattcag
1834	cattttgatttgaaagcggcgtattgcgtttctgaagg
1835	ccttcagaaacgcaatacgccgctttcaaatcaaaatg
1836	gaaagcgtggtattgcgcttctgaaggatttgatgc
1837	gcatcaaatccttcagaagcgcaataccacgctttc
1838	gttttggatgatgtggcgaatgaaaattacaacg
1839	cgttgtaattttcattcgccacatcatccaaaac
1840	gatcattgtgacgacagccaaagacagtgttgcc
1841	ggcaacactgtctttggctgtcgtcacaatgatc
1844	gagttgagatcaagagcattatttgaaaaggtccc
1845	gggacctttcaaataatgctcttgatctcaactc

Mismatches are underlined in mutagenic primers

H840V, H840stop and H840Q were generated using overlap extension with sets of either wild-type primer FP872 or FP873 in combination with mutagenic primers FP1543/FP1544, FP1545/FP1546, FP1547/FP1548 and FP1581/FP1582, respectively. The resulting 3.8 kb products were digested with *Bsp*119I/*Eco*72I and cloned into pG74 cut with the same enzymes.pG104 was obtained by ligating a 3.3 kb *Bam*HI/*Sal*I digested Mi-1 PCR product that was amplified with FP1095 and FP211 into pGEX-4T-1 (GE Healthcare) digested *Bam*HI/*Xho*I. For construction of Mi-1$^{KT556/557AA}$ and Mi-1^{H840A}, pG104 was used as a template for circular mutagenesis (Hemsley et al., 1989). The mutations were introduced using primer sets FP1099/FP1102 and FP1100/FP1103 to create pG108 and pG109, respectively. An Eco72I/Bsp119I fragment was exchanged between pG108 or pG109 and pG74 to obtain Mi-1$^{KT556/557AA}$ and Mi-1^{H840A}.
For heterologous Mi-1 protein production in *E. coli* for rabbit immunization, plasmid pKG6210 (Keygene N.V.) containing genomic Mi-1 promoter and coding sequence was used to transfer a Mi-1 *Nco*I/*Bsm*I fragment into pAS2-1 (Clontech Laboratories) digested *Nco*I/*Sma*I to obtain pSE06. An *Msc*I/*Sal*I fragment from pSE06 was ligated in pGEX-KG (Guan and Dixon, 1991) digested *Sma*I/*Sal*I to obtain pG01.
Rpi-blb1 constructs are amplified using FP771 and FP793 from pBINPLUS-RGA2-blb (van der Vossen et al., 2003). Gateway adapters were added to the coding sequence using FP872 and FP873, and the product was cloned into pDONR207 via a Gateway BP reaction to create pO2. Mutation D475V was introduced using the megaprimer method (Ke and Madison, 1997). The megaprimer was generated using primers FP754 and FP755 and, after purification the fragment, was extended using FP756. The product was digested *Eco*RI/*Bgl*II, and this 1.6 kb insert is ligated in a 3-point ligation with pO2 fragments generated by *Eco*RI/*Pst*I and *Pst*I/*Bgl*II to obtain pDONR207 containing Rpi-blb1^{D475V} with an intact stop codon. The insert was transferred to binary vector CTAPi in a Gateway LR reaction (Invitrogen). Correct sequences of all clones was confirmed by sequencing.

***Agrobacterium*-mediated transient transformation and protein extraction.**
Agrobacterium tumefaciens strain GV3101(pMP90) (Koncz and Schell, 1986) was transformed with binary constructs (Takken et al., 2000) and grown to OD_{600}=0.8 in YEB medium supplemented with 20 µM acetosyringone and 10 mM MES pH 5.6. Cells were pelleted and resuspended in infiltration medium (1x MS, 10 mM MES pH 5.6, 2% w/v sucrose) and infiltrated at OD_{600}=0.2 (for I-2, Rx and Rpi-blb1 constructs) or 1 (for Mi-1 constructs) into four-weeks-old *Nicotiana benthamiana* leaves.
For protein extraction, nine independent leaves were harvested and pooled 24 hours after agroinfiltration and frozen in liquid nitrogen. After grinding the tissue, it was allowed to thaw in 2 ml protein extraction buffer per gram of tissue (25 mM Tris pH 7.5, 1 mM EDTA, 150 mM NaCl, 10% Glycerol, 5 mM DTT, 1 x Roche Complete protease inhibitor cocktail and 2% PVPP). Extracts were cleared by centrifugation at 12,000 krcf at 4º C for 10 minutes and the supernatant was passed over 4 layers of Miracloth to obtain a total protein lysate. Samples were mixed with Laemmli sample buffer, and equal amounts of total protein were run at 8% SDS-PAGE gels and blotted on PVDF membranes using semi-dry blotting. Equal loading was assayed by Ponceau S staining of Rubisco. 5% Skimmed milk powder was used as blocking agent.

Trypan blue staining
Leaves were boiled for 5 minutes in a 1:1 mixture of ethanol and 0.33 mg/ml trypan blue in lactophenol, and destained overnight in 2.5 g/ml chloral hydrate in dH_2O.

Multiple sequence alignment of the MHD motif
R protein sequences found in the NCBI database were aligned using the MacVector ClustalW analysis tool (Oxford Molecular Group). The aligned sequences are sorted according to a phylogenetic tree constructed by neighbour-joining and midpoint-rooting in MacVector.

Antibody production

Anti-I-2 was produced in rabbit by Eurogentec, Seraing, Belgium, against synthetic peptide FEKVPNPSKRNIEE, which maps just N-terminal of the MHD motif and is affinity purified.
pG01 was transformed to *E. coli* BL21 (DE3) and expression of fusion protein GST-Mi-1, amino acids 161-899, was induced by addition of IPTG. The fusion protein was isolated using glutathione sepharose (GE Healthcare). The Mi-1 part was released from the glutathione beads using biotinylated human thrombin (Sigma). Thrombin was subsequently removed using streptavidin beads (Stratagene). Immunization was performed by injecting twice 250 µg purified Mi-1 (aa 161-899) protein into two New Zealand White rabbits with a 12-week interval. 14 weeks after the first injection, serum was collected and analyzed for specific cross-reactivity to purified Mi-1 in comparison to the pre-immune sera. Serum showing the highest signal was used to detect Mi-1 in planta. For Western blot detection, both the Mi-1 antibody and the secondary antibody goat anti-rabbit (Rockland Inc.) are used in a dilution of 1:4000 in PBSt.

Structure-based multiple sequence alignment of the NB-ARC domain

We created a multiple sequence alignment of the following R proteins and related sequences from the UniProtKB database using the program MUSCLE (Edgar, 2004): human Apaf-1 (O14727), tomato I-2 (Q9XET3) and Mi-1 (O81137), potato Rx (Q9XGF5), wild potato Rpi-blb (Q7XBQ9), mouse-ear cress RPM1 (Q39214), RPS2 (Q42484) and RPS4 (Q9XGM3), TMV resistance protein N (Q40392), linseed L6 (Q40253), tomato NRC1 (A1X877), *N. benthamiana* NRG1 (Q4TVR0), and nematode CED-4 (P30429). The secondary structure assignment of the PDB structure of Apaf-1 (identifier 1z6t, chain A) was obtained from the DSSP database (http://www.cmbi.kun.nl/gv/dssp/) and added to the alignment. To predict the secondary structure of R-proteins, we contacted the protein structure prediction server PSIPRED (http://bioinf.cs.ucl.ac.uk/psipred/). We improved the alignment manually by minor adjustments based on structure prediction results and pairwise superposition of the PDB structures of Apaf-1 (identifier 1z6t, chain A) and CED-4 (identifier 2a5y, chain B). Since the relative spatial orientation of the otherwise well-conserved NB, ARC1 and ARC2 subdomains of Apaf-1 and CED-4 differs, we applied the FATCAT program for structure superposition (Ye and Godzik, 2003), which considers conformational flexibility. Subdomain borders were taken from (Albrecht and Takken, 2006). Shading of more than 60% physicochemically conserved residues was produced by GeneDoc (http://www.psc.edu/biomed/genedoc/).

3D structure model of I-2

Based on the structure-based multiple sequence alignment of the NB-ARC domain, a pairwise sequence-structure alignment of tomato R protein I-2 and human Apaf-1 was constructed and formed the input into the 3D-modeling server WHAT IF (Vriend, 1990). This server returned a full-atom structure model of the NB-ARC domain of I-2. The structure of Apaf-1 (PDB code 1z6t, chain A) comprises the residues 108-450 (UniProt sequence O14727) and is mapped on the I-2 residues 153-506 (UniProt sequence Q9XET3). Interatomic contacts (van der Waals interactions, salt bridges, hydrogen bonds) were calculated by the WHAT IF server (Vriend, 1990).
The protein structure image of the model was illustrated using PyMOL (http://www.pymol.org).

Supplementary data

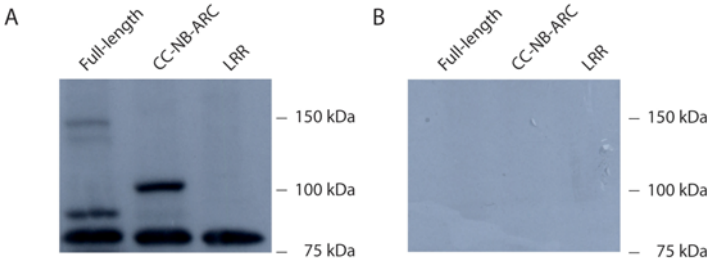

Figure S1

The Mi-1 antibody specifically recognizes transiently expressed Mi-1 protein. Western blots of 10 % SDS-PAGE gels loaded with total protein extracts of *Nicotiana benthamiana* leaves harvested 24 hours after agroinfiltration with constructs to express either full-length Mi-1, Mi-1 CC-NB-ARC, or Mi-1 LRR as indicated. One blot is probed with the Mi-1 antibody (**A**), the other with pre-immune serum (**B**). In both cases, peroxidase-linked goat anti-rabbit is used as a secondary antibody. Both full-length Mi-1 and Mi-1 CC-NB-ARC migrate according to their predicted molecular masses of ~145 and ~103 kDa.

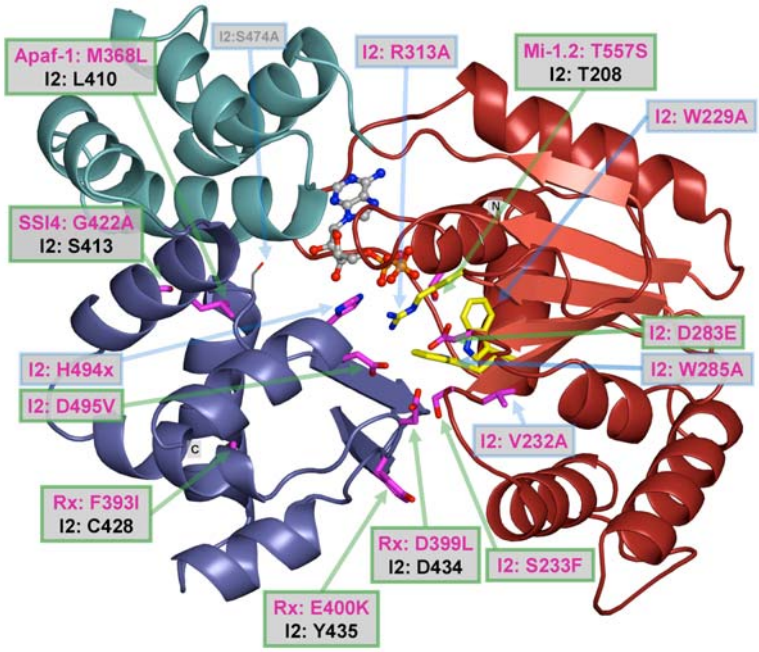

Figure S2

Structure model of the NB-ARC domain of I-2 indicates predicted important positions. Computationally derived 3D structure model of the NB-ARC domain of the resistance protein I-2. The model was created using the ADP bound structure of human Apaf-1 (PDB code 1z6t, chain A) as structural template for I-2. The protein name and the position of each mutation are indicated in magenta, the corresponding residues of I-2 are added in black. The locations of R protein mutations leading to HR are depicted as magenta sticks, leading to loss-of-function as yellow sticks. Mutations described in this study are framed in blue, otherwise in green. ADP atoms are depicted as balls-and-sticks. Subdomain coloring is: NB: red, ARC1: green, ARC2: blue. Atom coloring is: oxygen: red, nitrogen: blue, phosphorus: orange.

References

Albrecht, M., and Takken, F.L.W. (2006). Update on the domain architectures of NLRs and R proteins. Biochem Biophys Res Commun **339,** 459-462.

Ausubel, F.M. (2005). Are innate immune signaling pathways in plants and animals conserved? Nat Immunol **6,** 973-979.

Axtell, M.J., McNellis, T.W., Mudgett, M.B., Hsu, C.S., and Staskawicz, B.J. (2001). Mutational analysis of the *Arabidopsis RPS2* disease resistance gene and the corresponding *Pseudomonas syringae avrRpt2* avirulence gene. Mol Plant Microbe Interact **14,** 181-188.

Bendahmane, A., Farnham, G., Moffett, P., and Baulcombe, D.C. (2002). Constitutive gain-of-function mutants in a nucleotide binding site-leucine rich repeat protein encoded at the *Rx* locus of potato. Plant J **32,** 195-204.

Bent, A., and Mackey, D. (2007). Elicitors, Effectors, and R Genes: The New Paradigm and a Lifetime Supply of Questions. Annu Rev Phytopathol **45,** 399-436.

de la Fuente van Bentem, S., Vossen, J.H., de Vries, K.J., van Wees, S., Tameling, W.I.L., Dekker, H.L., de Koster, C.G., Haring, M.A., Takken, F.L.W., and Cornelissen, B.J.C. (2005). Heat shock protein 90 and its co-chaperone protein phosphatase 5 interact with distinct regions of the tomato I-2 disease resistance protein. Plant J **43,** 284-298.

Dinesh-Kumar, S.P., Tham, W.H., and Baker, B.J. (2000). Structure-function analysis of the tobacco mosaic virus resistance gene *N*. Proc Natl Acad Sci USA **97,** 14789-14794.

Edgar, R.C. (2004). MUSCLE: multiple sequence alignment with high accuracy and high throughput. Nucleic acids res **32,** 1792-1797.

Gabriëls, S.H.E.J., Takken, F.L.W., Vossen, J.H., de Jong, C.F., Liu, Q., Turk, S.C., Wachowski, L.K., Peters, J., Witsenboer, H.M., de Wit, P.J.G.M., and Joosten, M.H.A.J. (2006). cDNA-AFLP combined with functional analysis reveals novel genes involved in the hypersensitive response. Mol Plant Microbe Interact **19,** 567-576.

Gabriëls, S.H.E.J., Vossen, J.H., Ekengren, S.K., van Ooijen, G., Abd-El-Haliem, A.M., van den Berg, G.C.M., Rainey, D.Y., Martin, G.B., Takken, F.L.W., de Wit, P.J.G.M., and Joosten, M.H.A.J. (2007). An NB-LRR protein required for HR signalling mediated by both extra- and intracellular resistance proteins. Plant J **50,** 14-28.

Grant, M.R., Godiard, L., Straube, E., Ashfield, T., Lewald, J., Sattler, A., Innes, R.W., and Dangl, J.L. (1995). Structure of the Arabidopsis *RPM1* gene enabling dual specificity disease resistance. Science **269,** 843-846.

Guan, K.L., and Dixon, J.E. (1991). Eukaryotic proteins expressed in Escherichia coli: an improved thrombin cleavage and purification procedure of fusion proteins with glutathione S-transferase. Anal biochem **192,** 262-267.

Guenther, B., Onrust, R., Sali, A., O'Donnell, M., and Kuriyan, J. (1997). Crystal structure of the delta' subunit of the clamp-loader complex of E. coli DNA polymerase III. Cell **91,** 335-345.

Hellens, R., Mullineaux, P., and Klee, H. (2000). Technical Focus:a guide to *Agrobacterium* binary Ti vectors. Trends Plant Sci **5,** 446-451.

Hemsley, A., Arnheim, N., Toney, M.D., Cortopassi, G., and Galas, D.J. (1989). A simple method for site-directed mutagenesis using the polymerase chain reaction. Nucleic acids res **17,** 6545-6551.

Higuchi, R., Krummel, B., and Saiki, R.K. (1988). A general method of *in vitro* preparation and specific mutagenesis of DNA fragments: study of protein and DNA interactions. Nucleic acids res **16,** 7351-7367.

Howles, P., Lawrence, G., Finnegan, J., McFadden, H., Ayliffe, M., Dodds, P., and Ellis, J. (2005). Autoactive alleles of the flax *L6* rust resistance gene induce non-race-specific rust resistance associated with the hypersensitive response. Mol Plant Microbe Interact **18,** 570-582.

Hwang, C.F., Bhakta, A.V., Truesdell, G.M., Pudlo, W.M., and Williamson, V.M. (2000). Evidence for a role of the N terminus and leucine-rich repeat region of the *Mi* gene product in regulation of localized cell death. Plant Cell **12,** 1319-1329.

Jones, J.D.G., and Dangl, J.L. (2006). The plant immune system. Nature **444,** 323-329.

Ke, S.H., and Madison, E.L. (1997). Rapid and efficient site-directed mutagenesis by single-tube 'megaprimer' PCR method. Nucleic acids res **25,** 3371-3372.

Koncz, C., and Schell, J. (1986). The promoter of Tl-DNA gene *5* controls the tissue-specific expression of chimaeric genes carried by a novel type of *Agrobacterium* binary vector. Mol Gen Genet **204,** 383-396.

Leipe, D.D., Koonin, E.V., and Aravind, L. (2004). STAND, a class of P-loop NTPases including animal and plant regulators of programmed cell death: multiple, complex domain architectures, unusual phyletic patterns, and evolution by horizontal gene transfer. J Mol Biol **343,** 1-28.

Martin, G.B., Bogdanove, A.J., and Sessa, G. (2003). Understanding the functions of plant disease resistance proteins. Annu Rev Plant Biol **54,** 23-61.

Mestre, P., and Baulcombe, D.C. (2006). Elicitor-mediated oligomerization of the tobacco N disease resistance protein. Plant Cell **18,** 491-501.

Meyers, B.C., Dickerman, A.W., Michelmore, R.W., Sivaramakrishnan, S., Sobral, B.W., and Young, N.D. (1999). Plant disease resistance genes encode members of an ancient and diverse protein family within the nucleotide-binding superfamily. Plant J **20,** 317-332.

Meyers, B.C., Chin, D.B., Shen, K.A., Sivaramakrishnan, S., Lavelle, D.O., Zhang, Z., and Michelmore, R.W. (1998). The major resistance gene cluster in lettuce is highly duplicated and spans several megabases. Plant Cell **10,** 1817-1832.

Moffett, P., Farnham, G., Peart, J., and Baulcombe, D.C. (2002). Interaction between domains of a plant NBS-LRR protein in disease resistance-related cell death. EMBO J **21,** 4511-4519.

Müller, C.W., and Schulz, G.E. (1992). Structure of the complex between adenylate kinase from Escherichia coli and the inhibitor Ap5A refined at 1.9 Å resolution. A model for a catalytic transition state. J Mol Biol **244,** 159-177.

Ogura, T., and Wilkinson, A.J. (2001). AAA+ superfamily ATPases: common structure--diverse function. Genes Cells **6,** 575-597.

Ogura, T., Whiteheart, S.W., and Wilkinson, A.J. (2004). Conserved arginine residues implicated in ATP hydrolysis, nucleotide-sensing, and inter-subunit interactions in AAA and AAA+ ATPases. J Struct Biol **146,** 106-112.

Pan, Q., Liu, Y.S., Budai Hadrian, O., Sela, M., Carmel Goren, L., Zamir, D., and Fluhr, R. (2000). Comparative genetics of nucleotide binding site-leucine rich repeat resistance gene homologues in the genomes of two dicotyledons: tomato and *Arabidopsis*. Genetics **155,** 309-322.

Peart, J.R., Mestre, P., Lu, R., Malcuit, I., and Baulcombe, D.C. (2005). NRG1, a CC-NB-LRR protein, together with N, a TIR-NB-LRR protein, mediates resistance against Tobacco Mosaic Virus. Curr Biol **15,** 968-973.

Rairdan, G., and Moffett, P. (2007). Brothers in arms? Common and contrasting themes in pathogen perception by plant NB-LRR and animal NACHT-LRR proteins. Microbes Infect **9,** 677-686.

Rairdan, G.J., and Moffett, P. (2006). Distinct domains in the ARC region of the potato resistance protein Rx mediate LRR binding and inhibition of activation. Plant Cell **18,** 2082-2093.

Riedl, S.J., and Salvesen, G.S. (2007). The apoptosome: signalling platform of cell death. Nature rev **8,** 405-413.

Riedl, S.J., Li, W., Chao, Y., Schwarzenbacher, R., and Shi, Y. (2005). Structure of the apoptotic protease-activating factor 1 bound to ADP. Nature **434,** 926-933.

Rohila, J.S., Chen, M., Cerny, R., and Fromm, M.E. (2004). Improved tandem affinity purification tag and methods for isolation of protein heterocomplexes from plants. Plant J **38,** 172-181.

Salmeron, J.M., Oldroyd, G.E.D., Rommens, C.M.T., Scofield, S.R., Kim, H.S., Lavelle, D.T., Dahlbeck, D., and Staskawicz, B.J. (1996). Tomato *Prf* is a member of the leucine-rich repeat class of plant disease resistance genes and lies embedded within the *Pto* kinase gene cluster. Cell **86,** 123-133.

Sun, Q., Collins, N.C., Ayliffe, M., Smith, S.M., Drake, J., Pryor, T., and Hulbert, S.H. (2001). Recombination between paralogues at the *rp1* rust resistance locus in maize. Genetics **158,** 423-438.

Takken, F.L.W., Albrecht, M., and Tameling, W.I.L. (2006). Resistance proteins: molecular switches of plant defence. Curr Opin Plant Biol **9,** 383-390.

Takken, F.L.W., Luderer, R., Gabriëls, S.H.E.J., Westerink, N., Lu, R., de Wit, P.J.G.M., and Joosten, M.H.A.J. (2000). A functional cloning strategy, based on a binary PVX-expression vector, to isolate HR-inducing cDNAs of plant pathogens. Plant J **24,** 275-283.

Tameling, W.I.L., Elzinga, S.D., Darmin, P.S., Vossen, J.H., Takken, F.L.W., Haring, M.A., and Cornelissen, B.J.C. (2002). The tomato *R* gene products I-2 and Mi-1 are functional ATP binding proteins with ATPase activity. Plant Cell **14,** 2929-2939.

Tameling, W.I.L., Vossen, J.H., Albrecht, M., Lengauer, T., Berden, J.A., Haring, M.A., Cornelissen, B.J.C., and Takken, F.L.W. (2006). Mutations in the NB-ARC domain of I-2 that impair ATP hydrolysis cause autoactivation. Plant Physiol **140,** 1233-1245.

Tao, Y., Yuan, F., Leister, R.T., Ausubel, F.M., and Katagiri, F. (2000). Mutational analysis of the Arabidopsis nucleotide binding site-leucine- rich repeat resistance gene *RPS2*. Plant Cell **12,** 2541-2554.

Ting, J.P., Kastner, D.L., and Hoffman, H.M. (2006). CATERPILLERs, pyrin and hereditary immunological disorders. Nat Rev Immunol **6,** 183-195.

Tornero, P., Chao, R.A., Luthin, W.N., Goff, S.A., and Dangl, J.L. (2002). Large-scale structure-function analysis of the *Arabidopsis* RPM1 disease resistance protein. Plant Cell **14,** 435-450.

van der Biezen, E.A., and Jones, J.D.G. (1998). The NB-ARC domain: a novel signalling motif shared by plant resistance gene products and regulators of cell death in animals. Curr Biol **8,** R226-228.

van der Vossen, E., Sikkema, A., Hekkert, B.L., Gros, J., Stevens, P., Muskens, M., Wouters, D., Pereira, A., Stiekema, W., and Allefs, S. (2003). An ancient R gene from the wild potato species Solanum bulbocastanum confers broad-spectrum resistance to Phytophthora infestans in cultivated potato and tomato. Plant J **36,** 867-882.

van Ooijen, G., van den Burg, H.A., Cornelissen, B.J.C., and Takken, F.L.W. (2007). Structure and function of resistance proteins in solanaceous plants Annu Rev Phytopathol **45,** 43-72.

Vriend, G. (1990). WHAT IF: a molecular modeling and drug design program. J Mol Graphics **8,** 52-56, 29.

Yan, N., Chai, J., Lee, E.S., Gu, L., Liu, Q., He, J., Wu, J.W., Kokel, D., Li, H., Hao, Q., Xue, D., and Shi, Y. (2005). Structure of the CED-4-CED-9 complex provides insights into programmed cell death in *Caenorhabditis elegans*. Nature **437,** 831-837.

Ye, Y., and Godzik, A. (2003). Flexible structure alignment by chaining aligned fragment pairs allowing twists. Bioinformatics **19 Suppl 2,** II246-II255.